A Geometry Based Stochastic Model for MIMO V2V Channel Simulation in Cross-Junction Scenario

Theodorakopoulos, Andreas; Papaioannou, Panagiotis; Abbas, Taimoor; Tufvesson, Fredrik

Published in:
13th International Conference on ITS Telecommunications

2013

A Geometry Based Stochastic Model for MIMO V2V Channel Simulation in Cross-Junction Scenario

Andreas Theodorakopoulos† Panagiotis Papaioannou†
Taimoor Abbas* and Fredrik Tufvesson*
Department of Electrical and Information Technology, Lund University
Box 118, SE-22100, Lund, Sweden
Emails: [wir12ath, wir12ppa]@student.lu.se†, [taimoor.abbas, fredrik.tufvesson]@eit.lth.se*

***Abstract*—In this paper a multiple-input multiple-output (MIMO) simulation model for vehicle-to-vehicle (V2V) communication channels in an urban cross-junction scenario is presented. The model is an extension and modification of an existing T-junction model in the literature. Four propagation processes are considered: line-of-sight (LOS), single bounce reflections from side walls, double bounce reflections from side walls, and single bounce reflections from the corner of the building in front of the transmitter (TX) and receiver (RX). Each propagation process is linked to a cluster of scatterers, with a cluster size that varies with respect to the position of the TX and RX. The relations between angle-of-arrivals and angle-of-departures of all Multipath Components (MPCs) are derived depending on the different positions of the TX and RX. For the single bounce reflections from the corner a new method is being used where the scatterers are distributed randomly in a triangular plane, based on the assumption that corners of buildings typically have different scattering objects contributing to the reflection process. A complete expression for the time-variant transfer function is then derived by super positioning all contributions, including the LOS when this is available. The final results show that our model follows a realistic measurement based path-loss model, which subsequently makes the model a suitable candidate for analyzing MIMO V2V fading channels in cross-junction scattering environments.**

I. Introduction

Vehicle-to-vehicle (V2V) communications is a promising technology which will increase the efficiency of the traffic flow, reduce the number of road accidents and provide the basis for intelligent transportation systems [1]. The fundamental difference from a radio channel point of view when compared to traditional mobile communication is that both the transmitter (TX) and the receiver (RX) are moving. There are several measurement based studies and theoretical studies dedicated to V2V communications analyzing the statistical properties of the channel and mathematical representation of it [2]–[4]. The channel conditions in V2V communication scenarios can be extremely dynamic and single-input single-output (SISO) systems may not be an appropriate choice for a reliable reception in such scenarios. For that reason multiple-input multiple-output (MIMO) technology should also be considered in order to provide increased diversity and therefore higher robustness in the whole system [5].

A large number of measurement campaigns dedicated to V2V communication have been conducted to characterize MIMO channels around the $5.9\,\mathrm{GHz}$ frequency [7]–[9]. Moreover, several types of theoretical channel models have been proposed for analyzing V2V communications environments, like the two-ring MIMO V2V channel model described in [10]–[12], the geometrical street scattering model for a straight road in [13], the geometrical model for a corner junction in [14] and the T-junction scattering model that is presented in [15], [16]. Although these models are useful for a performance analysis of mobile-to-mobile (M2M) communication, they do not always cover all the different important scattering environments and cannot be applied to every street geometry like, e.g., a four-way cross-junction. Intersections in urban areas are quite common and usually constitute a place where frequent car accidents can happen, which justifies the need for a channel model of this scenario. Therefore, in this work we use the modeling concepts from the T-junction model and extend it for four way cross-junction.

In this paper, we propose a novel geometry based stochastic channel model (GSCM) for MIMO V2V channel simulations in an urban cross-junction scattering environment. To the author's best knowledge there is no other (GSCM) presented in the past to model a V2V cross-junction scattering environment using a similar approach. In our model both line-of-sight (LOS) and non-line-of-sight (NLOS) propagation are assumed, and both single and double bounce reflections are considered in the model. We take into account three clusters placed at realistic positions based on the experiences gained from real measurements. The first two clusters are located at the sides of the streets in which TX and RX are moving while the corner of the building located in front of the TX and RX, which is exactly on the opposite side of TX/RX streets, is considered to be the third cluster. For this third cluster we distribute the scatterers randomly in a triangular plane, with the assumption that corners of buildings typically have different scattering objects contributing to the reflection process and to add randomness needed for the channel model.

The geometry of a street intersection described by the cross-junction model is depicted in Fig. 1(a)-1(c). From the geometry of the model we derive exact expressions for the angle-of-arrival (AOA) and angle-of-departure (AOD), which are crucial for the channel characteristics.

Moreover, the space-time-frequency cross-correlation function (STF-CCF), the spatial CCF, the temporal auto-correlation function (ACF) and the frequency-correlation function (FCF)

are also derived. The power-delay-profile (PDP) and the normalized channel gain are derived from numerical simulations. The results on correlation functions are however left for future analysis therefore not included in this paper.

The structure of the paper is as follows. In Section II the geometrical scattering model for the cross-junction is introduced.The MIMO channel simulator is derived in section III by following the methodology in [15], [16] and changing the model appropriately for the cross-junction scattering environments. In the following section IV we present the numerical simulation results. Finally, in Section V conclusions are given.

II. The Geometric Cross-junction Scattering Model

The locations of the scatterers are of utmost importance for the statistical properties of the fading channel, and their position around the TX and RX play a very important role. Having said that, it is quite important to geometrically approach the problem in such a way that it would be realistic and would describe the environment in an appropriate way. As reality cannot be described in a totally perfect way, the geometrical approach should be as close as possible but simple enough to be processed.

The cross-junction propagation model is based on the previously mentioned T-junction model [15] that is specifically designed for three-way street junctions. The four-way cross-junction model in this paper is an extension of the T-junction model. In this work we do not only extend the model but also use realistic parameters for numerical simulations.

The geometry that is used for our study, to generalize a cross-junction in an urban area, is shown in Fig. 1(a)-1(c). The TX and RX vehicles are assumed to be at positions $O_T(0, -h_1^R - D_y)$ and $O_R(h_2^T + D_x, 0)$ moving towards the junction $O(0,0)$, which is the centre point of the referred geometry, with velocities ν_T and ν_R, respectively. The TX and the RX have M_T and M_R element antenna arrays, respectively.

In reality, scatterers exist along all sides of the streets but for simplicity we take three main clusters that contribute most to the received power based on experience gained from real V2V channel measurements.A first cluster comes from the scatterers close to the TX denoted by S_m^T for $m = 1, 2, ..., M$, which is used in the single bounce close to the TX (SBT). A second cluster comes from the scatterers found close to the RX denoted by S_n^T for $n = 1, 2, ..., N$, which is used for the single bounce close to the RX (SBR). Double bounce (DB) reflections arriving at the RX, defined as the MPCs that bounce on the SBT cluster as well on the SBR clusters, are also considered and are shown in Fig. 1(b) (for more information see [18]).

Furthermore, a third cluster comes from a single bounce reflection process from the corner (SBC) that is added in the model as shown in Fig. 1(c). The scatterers denoted by S_k^C for $k = 1, 2, ..., K$ are assumed to be uniformly randomly distributed in a triangle at the corner located in the front direction of the TX and the RX vehicles. The corner is formed at each time instant with respect to the position of the vehicles by drawing sight lines starting from the vehicles to the edges

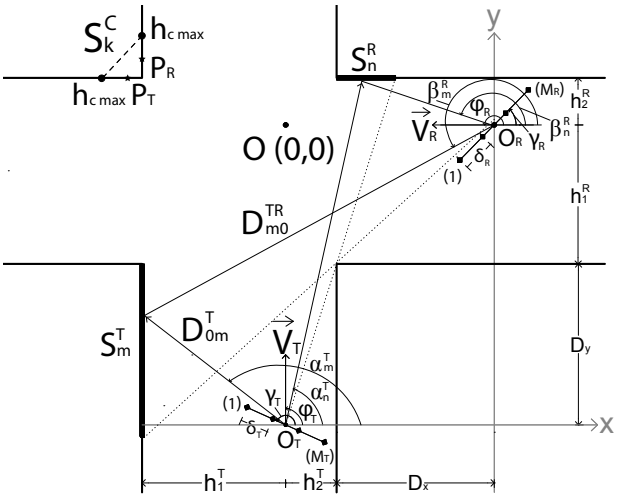

(a) Single-Bounce (SB)

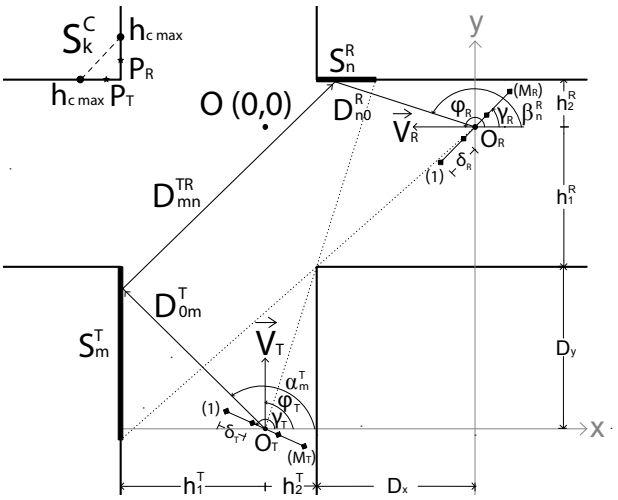

(b) Double-Bounce (DB)

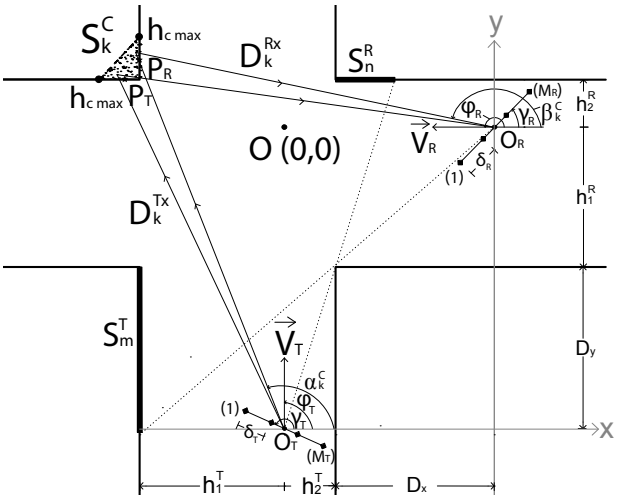

(c) Single-Bounce from corner (SBC)

Fig. 1. The geometry of the Cross-junction scattering model depicting; (a) the single-bounce mechanism, (b) the double-bounce mechanism, and (c) the single-bounce mechanism created by the corner.

of the side buildings to the building at the opposite corner as shown in Fig. 1(c). A threshold h_{cmax} is set in order to assure that the reflection is coming from the actual corner and not from scatterers very far away. From the geometry of the model then, the angles and the distances are calculated using the coordinates from both scatterer and vehicle, with a reference point given by O.

III. The Stochastic MIMO V2V Channel Simulation Model

For the channel simulation model, finite numbers of scatterers are chosen as in [16]. The time-variant transfer function of the channel is composed of the superposition of five partial transfer functions [17] given by (1) below,

$$\begin{aligned}\widehat{H}_{pq}(f',t) &= \widehat{H}_{LOS}(f',t)+\widehat{H}_{pq}^{SBT}(f',t)\\ &\quad+\widehat{H}_{pq}^{SBR}(f',t)+\widehat{H}_{pq}^{SBC}(f',t)\\ &\quad+\widehat{H}_{pq}^{DB}(f',t),\end{aligned} \tag{1}$$

where,

$$\begin{aligned}\widehat{H}_{LOS}(f',t) &= \sqrt{d_{decay_{LOS}}}\cdot e^{-j\frac{2\pi}{\lambda}d_{LOS}}\\ &\quad\cdot e^{-j2\pi f'\tau'_{LOS}}\cdot e^{j\left(f_{LOS}^{T}+f_{LOS}^{R}\right)t},\end{aligned} \tag{2}$$

$$\begin{aligned}\widehat{H}_{pq}^{SBT}(f',t) &= \sum_{m=1}^{M}\sqrt{d_{TX_m}}d_m^T a_m^T b_m^T\\ &\quad\cdot e^{j\left[\theta_m+\left(f_m^T+f_m^R\right)t\right]}\cdot e^{-j2\pi f'\tau'_{pmnq}},\end{aligned} \tag{3}$$

$$\begin{aligned}\widehat{H}_{pq}^{SBR}(f',t) &= \sum_{n=1}^{N}\sqrt{d_{RX_n}}d_n^R a_n^R b_n^R\\ &\quad\cdot e^{j\left[\theta_n+\left(f_n^T+f_n^R\right)t\right]}\cdot e^{-j2\pi f'\tau'_{pnq}},\end{aligned} \tag{4}$$

$$\begin{aligned}\widehat{H}_{pq}^{SBC}(f',t) &= \sum_{k=1}^{K}\sqrt{d_{C_k}}d_k^C a_k^C b_k^C\\ &\quad\cdot e^{j\left[\theta_k+\left(f_k^T+f_k^R\right)t\right]}\cdot e^{-j2\pi f'\tau'_{pkq}},\end{aligned} \tag{5}$$

$$\begin{aligned}\widehat{H}_{pq}^{DB}(f,t) &= \sum_{m=1}^{M}\sum_{n=1}^{N}\sqrt{d_{DB_{mn}}}d_{mn}^{TR}a_m^T b_n^R\\ &\quad\cdot e^{j\left[\theta_{mn}+\left(f_m^T+f_n^R\right)t\right]}\cdot e^{-j2\pi f'\tau'_{pmnq}},\end{aligned} \tag{6}$$

and their components are,

$$d_m^T = e^{-j\frac{2\pi}{\lambda}\left(\frac{h_1^T}{-\cos(\alpha_m^T)}+\frac{h_1^T+h_2^T+D_x}{-\cos(\beta_m^T)}\right)}, \tag{7}$$

$$d_n^R = e^{-j\frac{2\pi}{\lambda}\left(\frac{h_2^R}{\sin(\beta_m^T)}+\frac{h_1^R+h_2^R+D_y}{\sin(\alpha_n^R)}\right)}, \tag{8}$$

$$d_{mn}^{TR} = e^{-j\frac{2\pi}{\lambda}\left(\frac{h_1^T}{-\cos(\alpha_m^T)}+\frac{h_2^R}{\sin(\beta_n^R)}+D_{mn}^{TR}\right)}, \tag{9}$$

$$d_k^C = e^{-j\frac{2\pi}{\lambda}\cdot(D_k^{Rx}+D_k^{Tx})}, \tag{10}$$

$$a_m^T = e^{j\frac{2\pi}{\lambda}(M_T-2p+1)\frac{\delta_T}{2}\cos(\alpha_m^T-\gamma_T)}, \tag{11}$$

$$a_n^R = e^{j\frac{2\pi}{\lambda}(M_T-2p+1)\frac{\delta_T}{2}\cos(\alpha_n^R-\gamma_T)}, \tag{12}$$

$$a_k^C = e^{j\frac{2\pi}{\lambda}(M_T-2p+1)\frac{\delta_T}{2}\cos(\alpha_k^C-\gamma_T)}, \tag{13}$$

$$b_m^T = e^{j\frac{2\pi}{\lambda}(M_R-2q+1)\frac{\delta_R}{2}\cos(\beta_m^T-\gamma_R)}, \tag{14}$$

$$b_n^R = e^{j\frac{2\pi}{\lambda}(M_R-2q+1)\frac{\delta_R}{2}\cos(\beta_n^R-\gamma_R)}, \tag{15}$$

$$b_k^C = e^{j\frac{2\pi}{\lambda}(M_R-2q+1)\frac{\delta_R}{2}\cos(\beta_k^C-\gamma_R)}, \tag{16}$$

$$f_m^T = 2\pi f_{max}^T\cos\left(\phi_T-\alpha_m^T\right), \tag{17}$$

$$f_m^R = 2\pi f_{max}^R\cos\left(\phi_R-\beta_m^T\right), \tag{18}$$

$$f_n^T = 2\pi f_{max}^T\cos\left(\phi_T-\alpha_n^R\right), \tag{19}$$

$$f_n^R = 2\pi f_{max}^R\cos\left(\phi_R-\beta_n^R\right), \tag{20}$$

$$f_k^T = 2\pi f_{max}^T\cos\left(\phi_T-\alpha_k^C\right), \tag{21}$$

$$f_k^R = 2\pi f_{max}^R\cos\left(\phi_R-\beta_k^C\right), \tag{22}$$

$$\begin{aligned}D_{mn}^{TR} &= \{[D_x+h_1^T+h_2^T+h_2^R\cdot\cot(\beta_n^R)]^2\\ &\quad+[D_y+h_1^R+h_2^R+h_1^T\cdot\tan(\alpha_m^T)]^2\}^{\frac{1}{2}}.\end{aligned} \tag{23}$$

The τ'_{LOS}, τ'_{pmq}, τ'_{pnq}, τ'_{pkq} and τ'_{pmnq} are the propagation delays of the LOS, SBT, SBR, SBC and DB components from the p-th transmitting element to the q-th receiving element, respectively. In the following, we give the expressions for the propagation delays for all the cases, starting with τ'_{pmq}, $\tau'_{pmq}=D_{pmq}/c_0$ where D_{pmq} is the distance of the path traveled by the wave from the antenna element A_p^T to the antenna element A_q^R through the scatterer S_m^T. D_{pmq} is defined from the geometry of the intersection as

$$D_{pmq} = D_{pm}^T + D_{mq}^{TR}, \tag{24}$$

$$D_{pm}^T = D_{0m}^T - (M_T-2p+1))\frac{\delta_T}{2}\cos(\alpha_m^T-\gamma_T), \tag{25}$$

$$D_{mq}^{TR} = D_{m0}^{TR} - (M_R-2q+1))\frac{\delta_R}{2}\cos(\beta_m^T-\gamma_R), \tag{26}$$

where,

$$D_{0m}^{T} = -h_1^T / \cos(\alpha_m^T), \tag{27}$$

$$D_{m0}^{TR} = -(h_1^T + h_2^T + D_x)/\cos(\beta_m^T). \tag{28}$$

Similarly the delays τ'_{pnq} are given by $\tau'_{pnq} = D_{pnq}/c_0$, where D_{pnq} is the distance of the path traveled by the wave from the antenna element A_p^T to the antenna element A_q^R through the scatterer S_n^R. D_{pnq} is given as

$$D_{pnq} = D_{nq}^{R} + D_{pn}^{TR}, \tag{29}$$

$$D_{pn}^{TR} = D_{0n}^{TR} - (M_T - 2p + 1))\frac{\delta_T}{2}\cos(\alpha_n^R - \gamma_T), \tag{30}$$

$$D_{nq}^{R} = D_{n0}^{R} - (M_R - 2q + 1))\frac{\delta_R}{2}\cos(\beta_n^R - \gamma_R), \tag{31}$$

where

$$D_{0n}^{TR} = (h_1^R + h_2^R + D_y)/\sin(\alpha_n^R), \tag{32}$$

$$D_{n0}^{R} = h_2^R / \sin(\beta_n^R). \tag{33}$$

Likewise, the delays τ'_{pkq} are given by $\tau'_{pkq} = D_{pkq}/c_0$, where D_{pkq} is the distance of the path traveled by the wave from the antenna element A_p^T to the antenna element A_q^R through the scatterer S_k^C. D_{pkq} is given from the following expression as

$$D_{pkq} = D_{pk}^{T} + D_{kq}^{TR}, \tag{34}$$

$$D_{pk}^{T} = D_{0k}^{T} - (M_T - 2p + 1))\frac{\delta_T}{2}\cos(\alpha_k^C - \gamma_T), \tag{35}$$

$$D_{kq}^{TR} = D_{k0}^{TR} - (M_R - 2q + 1))\frac{\delta_R}{2}\cos(\beta_k^C - \gamma_R), \tag{36}$$

where

$$D_{0k}^{T} = D_{k}^{Tx} = \sqrt{(O_{T_x} - P_{Sc_x})^2 + (O_{T_y} - P_{Sc_y})^2} \tag{37}$$

$$D_{k0}^{TR} = D_{k}^{Rx} = \sqrt{(O_{R_x} - P_{Sc_x})^2 + (O_{R_y} - P_{Sc_y})^2}, \tag{38}$$

and where $P_{Sc_{x,y}}$ are the points of the scatterers distributed in the triangle, $O_{T_{x,y}}$ are the points of the Tx and $O_{T_{x,y}}$ are the points of Rx.

Finally, the propagation delays τ'_{pmnq} of the double bounce component are calculated from $\tau'_{pmnq} = D_{pmnq}/c_0$, where D_{pmnq} is the total distance travelled from the A_p^T antenna element to the A_q^R antenna element via the scatterers S_m^T and S_n^R. Then D_{pmnq} is given by

$$D_{pmnq} = D_{pm}^{T} + D_{mn}^{TR} + D_{nq}^{R}, \tag{39}$$

where D_{pm}^T, D_{mn}^{TR} and D_{nq}^R are given by (25), (23) and (31), respectively.

In all the partial transfer functions there is a squared multiplication factor $[d_{decay_{LOS}}, d_{TX_m}, d_{RX_n}, d_{C_k}, d_{DB_{mn}}]$ that represent the power decay of each multipath component coming from each scatterer depending on the distance it has traveled. Moreover, the phases θ_n θ_m θ_k and θ_{mn} are independent and identically distributed random variables uniformly distributed over $[0, 2\pi)$. The symbols α_m^T, α_n^R and α_k^C indicate the AODs while β_m^T, β_n^R and β_k^C indicate the AOAs. Moreover the γ_T and γ_R show the antenna tilt w.r.t. the x-axis at the TX and RX. The terms f_{max}^T and f_{max}^R are the maximum Doppler shifts affected by the movement of the TX and RX, respectively.

The calculation of the AOAs and AODs is based on the Riemann sum method (RSM) which is analyzed in [19]. Exact relationships are derived for the AOAs and AODs that are based on the geometry of the cross-junction model. The α_{max}^T and the α_{min}^T are derived for every position of the TX and RX. The scatterers are assumed not to remain in a constant position between packets transmitted, instead, they are redistributed in the cluster following every new TX/RX position. The same assumption applies for the α_{max}^R and α_{min}^R as,

$$\alpha_m^T = \alpha_{min}^T + \frac{\left|\alpha_{max}^T + \alpha_{min}^T\right|}{M}(m - 1/2), \tag{40}$$

for $m = 1, \ldots, M$ and $n = 1, \ldots, N$, where,

$$\alpha_n^R = \alpha_{min}^R + \frac{\left|\alpha_{max}^R + \alpha_{min}^R\right|}{N}(n - 1/2), \tag{41}$$

$$\alpha_{max}^T = \pi - \arctan\left(\frac{D_x \cdot D_y - h_1^R \cdot \left(h_1^T + h_2^T\right)}{D_x \cdot h_1^T}\right), \tag{42}$$

$$\alpha_{min}^T = \pi - \arctan\left(\frac{D_y}{h_1^T}\right), \tag{43}$$

$$\alpha_{max}^R = \arctan\left(\frac{D_y + h_1^R + h_2^R}{h_2^T}\right), \tag{44}$$

$$\alpha_{min}^R = \arctan\left(\frac{D_y}{h_2^T}\right). \tag{45}$$

The AOAs for the single-bounce components can be derived from the following expressions,

$$\beta_m^T = \pi + \arctan(\frac{h_1^R + D_y + h_1^T \cdot \tan(\alpha_m^T)}{h_1^T + h_2^T + D_x}), \tag{46}$$

$$\beta_n^R = \pi - \arctan\left(\frac{h_2^R \cdot \tan(\alpha_n^R)}{\tan(\alpha_n^R) \cdot (D_x + h_2^T) - (h_1^R + h_2^R + D_y)}\right). \tag{47}$$

For the double-bounce components, the RSM is used again to determine the α_m^T and β_n^R, with the only difference being the calculation of α_{min}^T, β_{max}^R and β_{min}^R. The α_m^T and β_n^R are given by the (48) and (49) as,

$$\alpha_m^T = \alpha_{min}^T + \frac{\left|\alpha_{max}^T + \alpha_{min}^T\right|}{M}(m - 1/2), \tag{48}$$

$$\beta_n^R = \beta_{min}^R + \frac{\left|\beta_{max}^R + \beta_{min}^R\right|}{N}(n - 1/2), \tag{49}$$

where $m = 1, \ldots, M$ and $n = 1, \ldots, N$. The α_{max}^{T} is given by (42) and the rest of the parameters are determined from the expressions below,

$$\alpha_{min}^{T} = \pi - \arctan\left(\frac{D_y}{h_1^T}\right), \tag{50}$$

$$\beta_{max}^{R} = \pi - \arctan\left(\frac{h_2^R}{D_x}\right), \tag{51}$$

$$\beta_{min}^{R} = \pi - \arctan\left(\frac{D_y \cdot h_2^R}{D_x \cdot D_y - h_2^T \cdot \left(h_1^R + h_2^R\right)}\right). \tag{52}$$

Finally, we derive the exact geometry of the corner by using coordinates referring to the junction as point $O(0,0)$. Points P_T and P_R are found by using straight line equations in order to define the three points of the triangle. The front corner of the triangle (vertex) will always be at $P_{C_{xy}}(-h_1^T, h_2^R)$. The next two coordinates $P_T(x,y)$ and $P_R(x,y)$ are defined as the points that can be found by the geometry using straight lines starting from the TX and the RX passing through the corners of the side buildings, situated close to the TX and RX, and ending at the building walls at the opposite corner, respectively.

For each position a check should be made so that $P_T(x) <= h_{cmax}$ and $P_R(y) <= h_{cmax}$. Each side of the triangle can have maximum length h_{cmax} in order to keep the corner cluster at a reasonable size. $P_T(y)$ and $P_R(x)$ are always static and equal to h_2^R and $-h_1^T$, respectively.

Then by using $P_T(x,y)$, $P_R(x,y)$ and $P_C(x,y)$ we define a triangle in which we uniformly randomly distribute K scatterers and together with the TX and RX we calculate the AOA and AOD that are used in the expressions mentioned before (13), (16), (22), (21), (35), (36) as,

$$\alpha_k^C = \pi + \arctan\left(\frac{P_k^{SC}(y) - O_T(y)}{P_k^{SC}(x) - O_T(x)}\right), \tag{53}$$

and

$$\beta_k^C = \pi + \arctan\left(\frac{P_k^{SC}(y) - O_R(y)}{P_k^{SC}(x) - O_R(x)}\right). \tag{54}$$

where $O_{T_{x,y}}$ and $O_{R_{x,y}}$ are the points of the TX and RX position respectively as defined in Section II and $P_k^{SC}(x,y)$ are the points of each scatterer S_k^C for $k = 1, 2, ..., K$ as aforementioned.

IV. Numerical Results

In the following part we present simulation results based on parameters described below. With a carrier frequency f_c of 5.9 GHz we get an approximate wavelength λ equal to 50.8 mm. The TX and RX speeds are set to 10 m/s which translates to 36 km/h and the directions of our moving terminals are $\phi_T = \pi/2$ and $\phi_R = \pi$.

The antenna orientations are $\gamma_T = 0$ and $\gamma_R = \pi/2$, respectively. Four elements were used for each antenna array at 1.5 m height from the ground and with a spacing of $\lambda/2$. Furthermore, the streets have a width of 20 m and distances

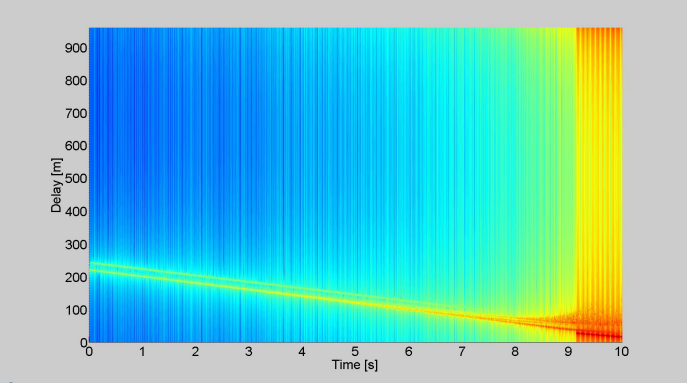

Fig. 2. The time variant Impulse Response H(τ,t) for channel 1 where elements $p = q = 1$

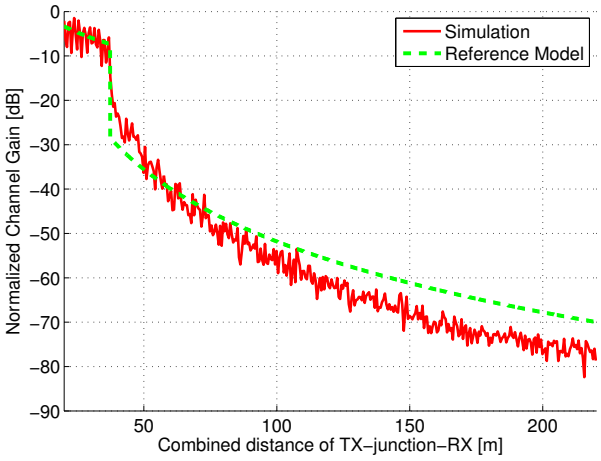

Fig. 3. Channel gains comparison for channel 1 where elements $p = q = 1$

to the left sides $h_1^T = h_1^R = 15$ m and to the right sides $h_2^T = h_2^R = 5$ m. The time sampling is set to $\Delta t = 2.5$ ms and the bandwidth was set to 240 MHz. Moreover the triangle threshold h_{cmax} in the corner was set to 5 m with $K = 50$ scatterers randomly distributed inside the triangular plane. The road side clusters are composed of $M = N = 70$ scatterers. Our frequency was separated into 769 frequency samples and we get 961 m maximum delay after the IFFT. We then simulate the power-delay profiles (PDPs) of the simulated time-variant channel transfer function. The PDPs are shown in Fig. 2, where we can clearly see the effect of LOS and can distinguish the contribution from the corner cluster from the other Multipath Components (MPCs) in the NLOS region, as it always comes with a larger delay due to the geometry. It is worth mentioning that the higher power seen at the end of the PDP (e.g., for delays exceeding 800 m) is due to artifacts introduced by the inverse Fourier transform of the transfer functions.

The normalized channel gain of our simulation model is then compared with the combined measurement based LOS and NLOS path-loss model from [21], which is validated in [22]. The reference power for each scatterer is then taken from [23], i.e., -5 dB for LOS and $-84 + 24\eta_p$ for each scattering component, where η_p is the path-loss exponent that is assumed

to be uniformly distributed as $\mathcal{U}[0, 3.5]$dB. The comparison of the channel gains is presented in Fig. 3.

In this comparison, it can be seen that the simulation gain fits nicely to the validated reference model. Nevertheless, a small difference can be spotted at the beginning of the line-of-sight, at approximately 30 m of combined distance from TX to RX through the junction. This is due to the fact that the reference model does not take into account the LOS and subsequently the diffraction that comes from the corner, which should make the transition smoother. Finally, after 100 meters a small difference can be noted between the two compared gains, which is due to the second or higher order scattering components that are not present in the simulation in order to avoid the high increase in both theoretical and computational complexity.

V. Conclusion

By starting with the T-Junction model a novel cross-junction model for multiple-input multiple-output (MIMO) vehicle-to-vehicle (V2V) channel simulation has been derived. A new cluster is added at the corner of the street intersection based on the experiences gained from the measurements that play a very important role in cross-junction environments. Moreover, the width of each cluster varies with respect to the position of the transmitter (TX) and receiver (RX). The power of each scatter is calculated from the measurement based model parameters. Finally, the proposed cross-junction simulation model appears to following the measurements based reference channel model, that makes cross-junction model a very good candidate for analyzing the V2V fading channel in four-way junctions in urban areas.

References

[1] F. Qu, F. Y. Wang, and L. Yang, "Intelligent transportation spaces: vehicles, traffic, communications, and beyond,"IEEE Communications Magazine, vol.48, no.11, pp.136–142, Nov. 2010

[2] C. S. Patel, G. L. Strüber, and T. G. Pratt, "Simulation of rayleigh-faded mobile-to-mobile communication channels," Communications, IEEE Transactions on, vol.53, no.10, pp.1773–1773, Oct. 2005

[3] A. S. Akki, and F. Haber, "A statistical model of mobile-to-mobile land communication channel," Vehicular Technology, IEEE Transactions on, vol.35, no.1, pp.2–7, Feb. 1986

[4] A. F. Molisch, F. Tufvesson, J. Karedal, and C. F. Mecklenbräuker, "A survey on vehicle-to-vehicle propagation channels," Wireless Communications Magazine, IEEE, vol.16, no.6, pp.12–22, 2009

[5] T. Abbas, J. Karedal, and F. Tufvesson, "Measurement-based analysis: The effect of complementary antennas and diversity on vehicle-to-vehicle communication," IEEE Antennas and Wireless Propagation Letters, vol.12, no.1, pp.309–312, 2013

[6] E. Talatar, "Capacity of multi-antenna Gaussian channels", European Transactions on Telecommunications, vol.10, no.6, pp.585–595, 1999

[7] L. Cheng, B. E. Henty, D. D. Stancil, F. Bai, and P. Mudalige, "Mobile vehicle-to-vehicle narrow-band channel measurement and characterization of the 5.9 GHz Dedicated Short Range Communication (DSRC) Frequency Band," Selected Areas in Communications, IEEE Journal on, vol.25, no.8, pp.1501–1516, Oct. 2007

[8] O. Renaudin, V. Kolmonen, P. Vainikainen, and C. Oestges, "Wideband MIMO car-to-car radio channel measurements at 5.3 GHz," Vehicular Technology Conference, 2008. VTC 2008-Fall. IEEE 68th, pp.1–5, 21-24 Sept. 2008

[9] J. Karedal, F. Tufvesson, T. Abbas, O. Klemp, A. Paier, L. Bernadó, and A. F. Molisch, "Radio channel measurements at street intersections for vehicle-to-vehicle safety applications," in IEEE VTC 71st Vehicular Technology Conference (VTC 2010-spring), May 2010.

[10] M. Pätzold, B. O. Hogstad, and N. Youssef, "Modeling, analysis, and simulation of MIMO mobile-to-mobile fading channels," Wireless Communications, IEEE Transactions on , vol.7, no.2, pp.510–520, Feb. 2008

[11] G. J. Byers, and F. Takawira, "Spatially and temporally correlated MIMO channels: modeling and capacity analysis," Vehicular Technology, IEEE Transactions on, vol.53, no.3, pp.634–643, May 2004

[12] Zhongwei Tang; Mohan, A.S., "A correlated indoor MIMO channel model," Electrical and Computer Engineering, 2003. IEEE CCECE 2003. Canadian Conference on, vol.3, pp.1889–1892 vol.3, 4-7 May 2003

[13] A. Chelli, and M. Pätzold, "A MIMO mobile-to-mobile channel model derived from a geometric street scattering model," Wireless Communication Systems, 2007. ISWCS 2007. 4th International Symposium on, pp.792–797, 17-19 Oct. 2007

[14] C. Wei, H. Zhiyi, and Y. Tianren, "A street reference model of MIMO vehicle-to-vehicle fading channel," Industrial Electronics and Applications, 2008. ICIEA 2008. 3rd IEEE Conference on, pp.275–278, 3-5 June 2008

[15] Z. He, W. Chen, W. Zhou, M. Pätzold, and A. Chelli, "Modelling of MIMO vehicle-to-vehicle fading channels in T-junction scattering environments," Antennas and Propagation, 2009. EuCAP 2009. 3rd European Conference on, pp.652–656, 23-27 March 2009

[16] W. Zhou, M. Pätzold, W. Chen, and Z. He, "An ergodic wideband MIMO channel simulator based on the geometrical T-junction scattering model for vehicle-to-vehicle communications," Communications and Electronics (ICCE), 2010 Third International Conference on, pp.323–328, 11-13 Aug. 2010

[17] B. O. Hogstad, and M. Pätzold, "On the stationarity of sum-of-cisoids-based mobile fading channel simulators," Vehicular Technology Conference, 2008. VTC Spring 2008. pp.400–404, 11-14 May 2008

[18] A. G. Zajic, G. L. Stuber, T. G. Pratt, and S. Nguyen, "Statistical modeling and experimental verification of wideband MIMO mobile-to-mobile channels in highway environments," Personal, Indoor and Mobile Radio Communications, 2008. PIMRC 2008. IEEE 19th International Symposium on, pp.1–5, 15-18 Sept. 2008

[19] C. A. Gutierrez, and M. Pätzold, "The design of sum-of-cisoids rayleigh fading channel simulators assuming non-isotropic scattering conditions," Wireless Communications, IEEE Transactions on, vol.9, no.4, pp.1308–1314, April 2010

[20] R. Osada, T. Funkhouser, B. Chazelle, and D. Dobkin, "Matching 3D models with shape distributions," Shape Modeling and Applications, SMI 2001 International Conference on., pp.154–166, May 2001

[21] T. Mangel, O. Klemp, H. Hartenstein, "A validated 5.9 GHz Non-Line-of-Sight path-loss and fading model for inter-vehicle communication," ITS Telecommunications (ITST), 2011 11th International Conference on, pp.75–80, 23-25 Aug. 2011

[22] T. Abbas, A. Thiel, T. Zemen, C. F. Mecklenbräuker and F. Tufvesson, "Validation of a non-line-of-sight path-loss model for V2V communications at street intersections", ITS Telecommunications (ITST), 2013 13th International Conference on, Tampere, Finalnd, 05-07 Nov. 2013

[23] J. Karedal, F. Tufvesson, N. Czink, A. Paier, C. Dumard, T. Zemen, C. F. Mecklenbrauker, and A. F. Molisch, "A geometry-based stochastic MIMO model for vehicle-to-vehicle communications," Wireless Communications, IEEE Transactions on, vol.8, no.7, pp.3646–3657, July 2009